Appl Phys B (2010) 101: 565–570
DOI 10.1007/s00340-010-4224-2

Applied Physics B
Lasers and Optics

Automated characterization and alignment of passively mode-locked fiber lasers based on nonlinear polarization rotation

T. Hellwig · T. Walbaum · P. Groß · C. Fallnich

Received: 16 June 2010 / Revised version: 12 August 2010 / Published online: 15 September 2010

Abstract We present for the first time to the best of our knowledge a computerized characterization and alignment scheme of an erbium all-fiber laser passively mode-locked by nonlinear polarization rotation. This scheme can replace the common trial and error alignment procedure with manual polarization controllers and therefore greatly reduce the time to start up an ultrashort pulsed fiber laser. Based on the mode-locking maps generated by automated characterization we also demonstrate reproducible selection of pulses with different pulse durations and central wavelengths. These settings were stable over several days allowing us to choose that pulsed operation mode that is more advantageous for a specific application.

1 Introduction

Passively mode-locked erbium fiber lasers are mechanically robust, cost-effective and reliable and thus attractive as possible turn-key devices for applications in nonlinear microscopy [1] or metrology [2]. Passive mode-locking is usually achieved utilizing saturable absorbers, nonlinear loop mirrors or nonlinear polarization rotation as mode-locking mechanisms [3–6]. Erbium fiber lasers passively mode-locked by nonlinear polarization rotation stand out due to their compact cavities, combining a very simple design with the shortest pulses demonstrated up to date [7, 8]. Polarization mode-locked fiber lasers include the well known soliton [9] and stretched-pulse [7] fiber lasers as well as dissipative soliton lasers [10], similariton lasers [11] and the recently discovered soliton–similariton lasers [12]. Unfortunately, self-starting mode-locking operation is often hard to achieve, leading to unpredictable alignment time. In order to improve the usability of such lasers as turn-key devices we want to present first results toward an automatic characterization and alignment scheme. This should reduce the alignment time and accomplish a better control of system parameters.

Mode-locked fiber lasers based on nonlinear polarization rotation utilize the intensity-dependent rotation of the polarization in combination with a polarizing element as a fast artificial saturable absorber for initiating and stabilizing the mode-locking process. Although these lasers have been in the focus of intense research and subject of a large number of publications there are only a few systematic studies on the dependence of mode-locking regimes on polarization [13, 14]. Within those studies an experimental cartography of mode-locking regimes with respect to the orientation of two half-wave plates before and after a polarizer was reported. Good agreement of these cartographies with a theoretical model obtained from two coupled nonlinear Schrödinger equations was shown. For this purpose only half-wave plates have been used thereby restricting the possible polarizations to a two dimensional parameter space instead of a four-dimensional one. Furthermore, the use of bulk wave plates relies on a free space section and therefore makes an all-fiber approach impossible. And, the mechanical rotation of wave plates makes rapid system characterization difficult thereby hindering a short alignment time.

The aim of this paper is to show an automated characterization of the polarization state and the alignment of an erbium-doped passively mode-locked all-fiber laser. We would like to demonstrate that a full control over the four-dimensional parameter space leads to a better control and optimization of system parameters like pulse duration, cen-

T. Hellwig (✉) · T. Walbaum · P. Groß · C. Fallnich
Institute of Applied Physics, Westfälische Wilhelms-Universität, Corrensstr. 2, 48149 Münster, Germany
e-mail: tim.hellwig@uni-muenster.de

tral wavelength and average output power. For this purpose we combine a home-built all-fiber division-of-amplitude polarimeter (Sect. 2.2) with an automatic polarization control based on piezoelectric squeezers in the cavity (Sect. 2.3). This new approach allows us to achieve a fast characterization of laser parameters in respect of polarization. In Sect. 3 results from the automated alignment and characterization are reported.

2 Experimental setup

2.1 Erbium fiber laser

Our setup is an unidirectional all-fiber ring laser (Fig. 1) containing 1.23 m of erbium-doped fiber (Liekki Er30-4/125). The erbium fiber is pumped in backward direction by a pump diode operating at 976 nm with a maximum output power of 500 mW. The polarization of the laser light is adjusted in front of a polarization dependent isolator (PDI) using a computer-controlled automatic polarization controller (APC, described in detail in Sect. 2.3). Unidirectional lasing is ensured by the PDI that also serves as the polarization discriminating element for achieving artificial saturable absorption. We use only one automatic polarization controller in this experiment and the initial state of polarization (SOP) behind the polarizing element is controlled with a conventional manual polarization controller (MPC) which turned out to be sufficient for a good control over laser parameters. One can imagine to replace the MPC with a second APC for fine tuning of the initial condition once a working point has been identified but must not forget that even with two APCs a full four-dimensional scan with a typical density of data points would take over a month for a single laser. This means regardless of the polarization control only a coarse scanning of the initial conditions is recommended.

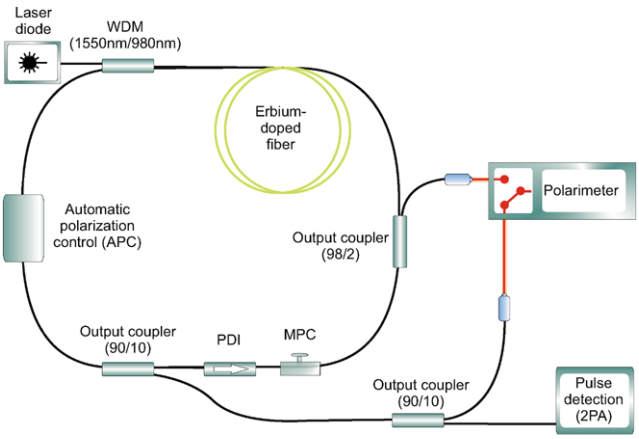

Fig. 1 Experimental setup (PDI: polarization dependent isolator; MPC: manual polarization controller; WDM: wavelength-division multiplexer; 2PA: two-photon absorption)

For analyzing the polarization as well as the mode-locking state, a fraction of the laser light is coupled out behind each polarization controller with fiber couplers. A few hundred μW are coupled into the division-of-amplitude polarimeter (DOAP, see Sect. 2.2 for details) for a polarization measurement while the rest is used for simultaneously measuring a two-photon absorption (2PA) signal on a silicon photodiode. As only the high peak power of an ultrashort pulse will lead to strong two-photon absorption, this signal can be used as an indicator for mode-locked operation. Optionally an interferometric autocorrelation trace was measured for each SOP with the drawback of increased measurement time.

The laser had a maximum output power of 8 mW at the 10% output coupler and a repetition frequency of about 45 MHz. The total second order dispersion of the cavity was calculated from spectral sidebands [15] to be $\beta_2^T = -(0.054 \pm 0.001)$ ps^2 at a central wavelength of 1556 nm.

2.2 All-fiber division-of-amplitude polarimeter

Because of the great number of measurement points for a characterization of the mode-locking regimes versus the polarization a fast measurement device is needed to achieve acceptable scanning times. Therefore, classical methods like the measurements with rotating retarder and fixed analyzer [16] are not applicable. Division-of-amplitude polarimeters [17] on the other hand can measure arbitrarily fast, being only limited by time constants of analog-to-digital conversion.

We designed an all-fiber DOAP based on commercially available telecommunication components similar to an in-line fiber optic polarimeter reported by Lee et al. [18]. Polarimeters based on fiber couplers are cost-effective, require low alignment and can be easily integrated into our all-fiber concept. The input laser light is distributed to eight fibers by means of a tree splitter (see Fig. 2). One fiber is used in combination with a photodiode (PD 8) to normalize the measured power of the laser light while the other seven are randomly bent to introduce different values of birefringence in each of them. Small polarizing filters are glued to the tip of the FC-PC fiber connectors at the end of the seven fibers and the light is detected behind each polarizer via a FC receptacle InGaAs photodiode (PD1 to PD7). In comparison with

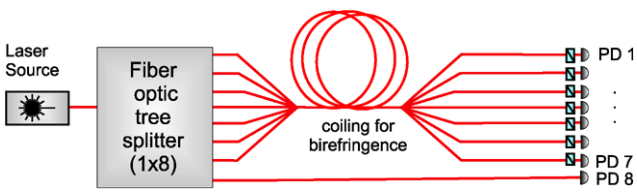

Fig. 2 Schematic sketch of the all-fiber division-of-amplitude polarimeter (PD: photodiode, for PD1 to PD7 with polarizer in front)

the in-line polarimeter of Lee et al. [18] we reduced the number of components and related costs to a minimum by using the random birefringence of the coiled fibers instead of a quarter-wave plate as well as cheap polarizing filters instead of optical-fiber polarizers. In the case of ideal photodetectors it would be sufficient to use a 1×5 coupler with four detectors (as in reference [18]) but in the presence of detector noise a 1×8 fiber coupler with seven polarization–sensitive detectors has the advantage of an over-determined system accomplishing the reduction of the rms error of the measured polarization as it was shown by Cui and Azzam [19].

A division-of-amplitude polarimeter can be treated as a black box with an unknown but linear dependence of the current values, I_1 to I_7, obtained from the seven PDs on the input polarization [20]. The dependence can therefore be expressed as a matrix multiplication between a vector of the four Stokes parameters S_0 to S_3

$$\begin{pmatrix} I_1 \\ \vdots \\ I_7 \end{pmatrix} = \mathbf{M} \cdot \begin{pmatrix} S_0 \\ S_1 \\ S_2 \\ S_3 \end{pmatrix} \tag{1}$$

with the 7×4 instrument matrix $\mathbf{M}$. The Stokes parameters are a set of four values describing the state of polarization including that of partially polarized light. After a calibration measurement to determine $\mathbf{M}$ [20, 21] the Stokes parameters can be obtained by multiplication of the PD current vector with the pseudo inverse matrix of $\mathbf{M}$.

The polarization measurements of the DOAP have been verified with the figure-of-eight test [21]. In this test the laser light is linearly polarized using a polarizing filter with a very high polarization extinction ratio (>10000:1) and the polarization is measured behind a quarter-wave plate (QWP). When the fast axis of the QWP is varied through 180° the resulting curve on the surface of the Poincaré sphere resembles an eight. In Fig. 3 the measured Stokes parameters are displayed. Good agreement between the measured data and the theoretical prediction from Mueller matrix calculus (solid curves in Fig. 3) was found. For a fixed incoming polarization the residual rms errors of the normalized Stokes parameters were below 0.001 for all four parameters.

2.3 Automatic polarization scanning

In order to control the polarization in a fiber one can utilize stress-induced birefringence. Squeezing a fiber between two parallel surfaces induces a linear birefringence that can be represented as a right-handed rotation of an input SOP on the surface of the Poincaré sphere [22]; the axis of rotation lies in the equatorial plane, and its azimuth angle is determined by twice the angle of the clamping force with respect to the laboratory system in the fiber. In practical terms the laboratory coordinate system is chosen in that way that the clamping direction of the first piezoelectric squeezer defines the zero azimuth angle (horizontal polarization).

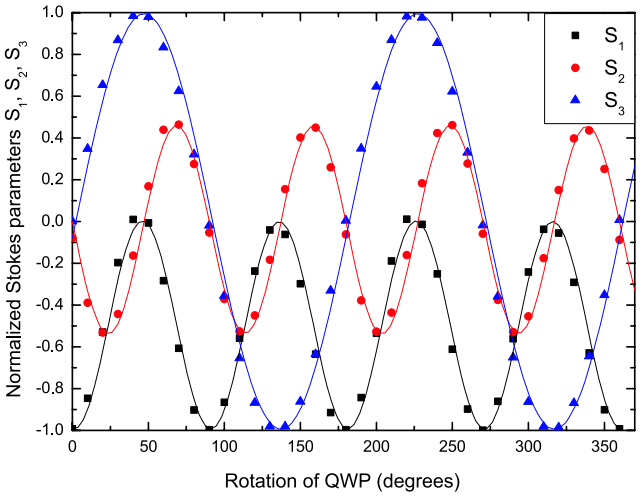

Fig. 3 Normalized Stokes parameters shown as a function of quarter-wave plate angle (figure-of-eight test). *Solid curves*: Expected values from the Mueller matrix calculus for linearly polarized light and variation of QWP fast axis through 360°. Measurement points from polarimeter

In our experiment the computerized polarization control is implemented with modularly constructed piezoelectric squeezers [22] allowing a birefringence-induced phase difference larger than 2π for each squeezer. Two subsequent squeezers with a difference of 45° in their clamping angle rotate an incident SOP on the surface of the Poincaré sphere with orthogonal axis of rotation. Therefore, scanning the applied voltages of the two squeezers allows covering the whole Poincaré sphere with a measurement grid for appropriate incoming SOP. The incoming SOP is not appropriate if its representation on the Poincaré sphere lies on the axes of rotation of the first squeezer. This means it is an eigenstate of polarization of that squeezer and squeezing the fiber in the direction of this squeezer has no effect on the incoming SOP. For that reason a third squeezer in front of the APC has to be used before each scan in order to adjust the polarization of the incoming laser light so that polarization eigenstates of the first piezoelectric squeezer are avoided. The waiting time between two data points on the measurement grid determines the available time for the laser to switch to pulsed operation. We have been aware of the starting dynamics of the fiber laser: In simulations of similar lasers starting from white noise a few thousand cavity round trips were found to be sufficient for convergence to pulsed operation [23]. This would amount to a necessary waiting time of only 0.1 ms, while in experimental investigations on the stochastic nature of the starting dynamics maximum probabilities for starting times of pulsed operation around 20 ms [24, 25] were found. Nevertheless, to limit the maximum measurement time of a scan for a single initial polarization

condition to 15 minutes an artificial waiting time of 10 ms was introduced. This leads to an average acquisition time of about 25 ms per data point with our characterization system and is a good compromise between a high probability that the laser will switch to pulsed operation, allowing the detection of even small mode-locking regions, and a fast acquisition time. An influence of the waiting time on mode-locking regions could be investigated in combination with a detailed study of the starting dynamics of the laser but is beyond the scope of this work.

We would like to note, that the measured polarization is usually not identical with the polarization in the laser cavity. This is due to intrinsic as well as bend-induced birefringence in the transport fibers to the DOAP. In principle only relative polarization changes are detectable. One can overcome this limitation with a self-referencing approach by evaluating the measured polarization changes after a scan. During a measurement the voltage of one piezoelectric squeezer is scanned repeatedly. Between each voltage scan the voltage of the other squeezer is increased. Therefore the measurement consists of circles on the Poincaré sphere determined by the axis of rotation of the scanned squeezer while the distance between the circles is determined by the voltage increment of the other squeezer. Utilizing this dependence of the measurement data on the clamping angle of the squeezer gives the possibility to correct for polarization changes of the transport fiber: the axis of rotation of the respective squeezer can be calculated by least square fitting a circle to the measured polarization changes from the scanned squeezer. The measured axes of rotation usually do not lie within the equatorial plane at the correct azimuth angles (zero and 90°) because of the birefringence of the transport fiber. Correcting this by simple coordinate transformation (using Euler rotation) converts the measured polarization into the intracavity polarization at the APC.

3 Results

We scanned the polarization with the APC for a fixed position of the manual polarization controller and measured the 2PA signal at each SOP. In order to investigate whether there are significant hysteresis effects in detecting mode-locking regions the scanning direction of the piezoelectric squeezers was reversed. Furthermore, the scanning order of the two squeezers was changed, thereby rotating the scanning direction by 90 degrees on the Poincaré sphere. During the fast scans no hysteresis in the detected mode-locking regimes was observed. Only small hysteresis was observable if a fine tuning of polarization was performed at a specific operation point. However, it had no influence in detecting the starting points of mode-locked operation. The result of a typical scan is shown in Fig. 4a, where the 2PA signal is displayed color-coded on the surface of the Poincaré sphere.

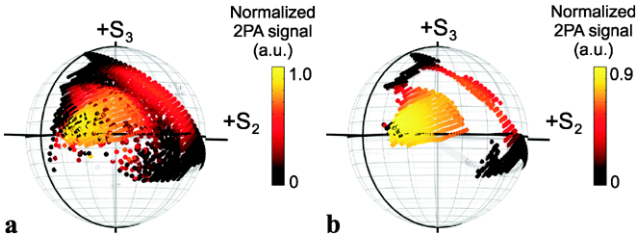

Fig. 4 Two-photon absorption signal color-coded on the Poincaré sphere wherever it exceeds the mode-locking threshold (**a**) without and (**b**) after numerical filtering of irregular pulses

Plotted are only the 2PA values, which are above a certain threshold, which has been experimentally verified to be the threshold for pulsed operation. Pulsed operation, however, does not only mean mode-locked operation of the erbium fiber laser, but also burst mode, q-switched, and hybrid operation. In order to distinguish between these cases, we have implemented a numerical filter function by calculating the standard deviation of the DOAP photodiode currents. The photodiodes act as a low pass filter with a cutoff frequency below the repetition rate of the laser. Therefore, the standard deviation is lowest for regular pulse trains of mode-locked operation. The result after applying this numerical filter is displayed in Fig. 4b. The large area of pulsed operation (Fig. 4a) is now reduced to two smaller areas of mode-locked operation, which are separated by an area, wherein q-switched as well as hybrid operation was observed.

In order to verify the coordinate transformation of our results, the orientation of the transportation fiber was changed and the scan repeated. Selectively plotting the 2PA signal color-coded on the Poincaré sphere where it exceeds the mode-locking threshold, reveals that the measurements resemble each other (Fig. 5a and b), but the coordinate system is rotated, as expected from the introduced birefringence difference. Applying the transformation discussed earlier (see Sect. 2.3) to the measurement data from Fig. 5a and b and thus representing both measurements in the same coordinate system yielded very good agreement (Fig. 5c and d), thereby approving the feasibility of the transformation into the mutual coordinate system of polarization. This ensures that even after a rearrangement or replacement of the polarimeter the measurements stay comparable to earlier ones.

In order to fully characterize the laser, the MPC was set to 44 different positions covering the Poincaré sphere in a coarse grid. This ensures a good coverage of possible initial conditions. At each position a full scan was performed using the APC, leading to a complete mode-locking map for each MPC position. Mode-locking regimes with different pulse characteristics were observed while varying the position of the MPC. In Fig. 6a the 2PA signal is displayed color-coded on the Poincaré sphere for a specific MPC position, in case it is above the threshold for pulsed operation. Leaving the MPC at this fixed position the same mode-locking

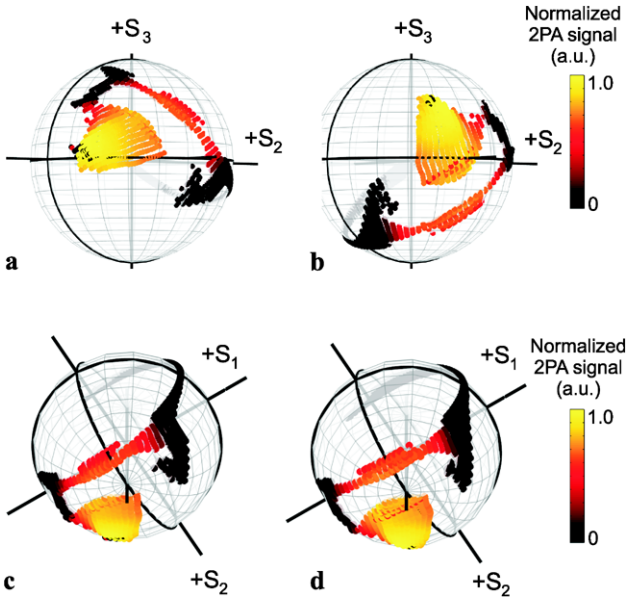

Fig. 5 Two-photon absorption (2PA) signal above the mode-locking threshold color-coded on the Poincaré sphere (**a**) before and (**b**) after rearranging the transportation fiber to the polarimeter. (**c**) Transformation of (**a**), and (**d**) transformation of (**b**) into the intracavity polarization coordinate system

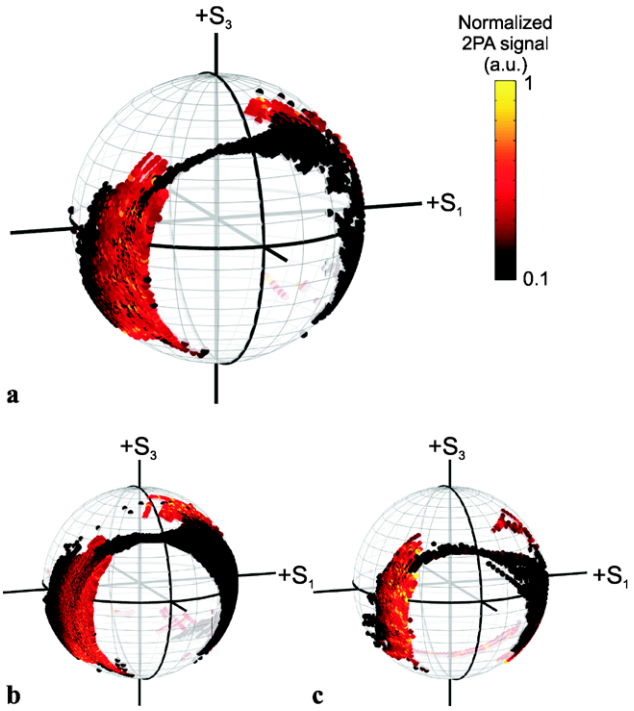

Fig. 6 Two-photon absorption signal color-coded on the Poincaré sphere (**a**) wherever it exceeds the mode-locking threshold for a fixed MPC position, (**b**) on the next day, and (**c**) after five days

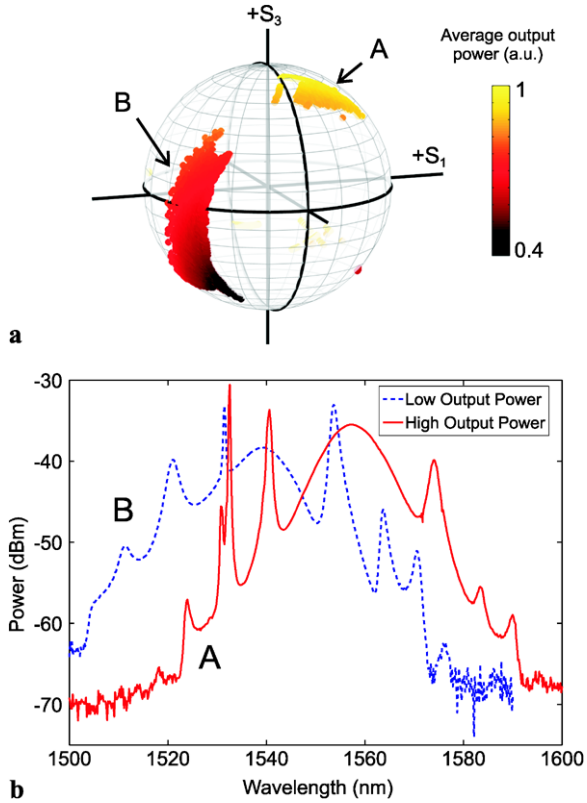

Fig. 7 (**a**) Average output power in the mode-locking regimes (color-coded on the Poincaré sphere when the two-photon signal indicated mode-locking). (**b**) The corresponding optical spectra were recorded when the laser was operating in the mode-locking regime with high output power (*solid curve*) and with lower output power (*broken curve*)

regimes could be reproduced over several days by scanning the APC despite climate changes within the lab as it is shown in Fig. 6b and c. In Fig. 7a the average output power of this mode-locking map is shown on the Poincaré sphere, displayed are only the two mode-locking regimes with the highest 2PA signal. All other mode-locking regimes were either unstable or showed—in case of a weak 2PA signal—narrow optical spectra indicating long pulses that were not measurable with the interferometric autocorrelator. The two mode-locking regimes of interest differed in average output power as well as in pulse duration and central wavelength. The mode-locking regime with higher output power (about 6 mW; upper right regime A in Fig. 7a) provided pulses with a pulse duration of 310 fs around a central wavelength of 1556 nm (solid curve in Fig. 7b) whereas the mode-locking regime B with lower average output power (about 2 mW to 5 mW) provided 250 fs pulses around a central wavelength of 1540 nm (broken curve in Fig. 7b).

This example demonstrates the advantage of performing a full scan of the polarization when adjusting an erbium fiber laser: without knowledge of the existence of the two separated mode-locking regimes as a function of polarization one might adjust the laser to operate in either one of the areas. In our experiment a specific selection of different pulse characteristics was possible allowing to operate the laser in the

mode that would be more advantageous for a specific application.

4 Summary and conclusion

In summary, we established for the first time to the best of our knowledge a method for the automated characterization and alignment of a passively mode-locked erbium fiber laser based on nonlinear polarization rotation. Our method combines a fast fiber-based division-of-amplitude polarimeter with a computerized polarization control based on piezoelectric squeezers. We obtained mode-locking maps regarding all possible polarizations by scanning the whole Poincaré sphere. Mode-locking regimes with different output power and pulse characteristics have been observed reproducibly and could be specifically selected by tuning only the polarization with the automatic polarization control. These results should enable an automatic adjustment and optimization of laser output characteristics in respect of pulse duration or peak power. In our on-going work, we will investigate a systematic tuning of the laser characteristics by polarization control in order to accomplish a precise stabilization of the mode-locked operation for precision, long-term and industrial applications, e.g. to compensate variations of birefringence introduced by linear or nonlinear effects.

References

1. G. Krauss, T. Hanke, A. Sell, D. Trautlein, A. Leitenstorfer, R. Selm, M. Winterhalder, A. Zumbusch, Opt. Lett. **34**, 2847 (2009)
2. H. Inaba, Y. Daimon, F.L. Hong, A. Onae, K. Minoshima, T.R. Schibli, H. Matsumoto, M. Hirano, T. Okuno, M. Onishi, M. Nakazawa, Opt. Express **14**, 5223 (2006)
3. L.E. Nelson, D.J. Jones, K. Tamura, H.A. Haus, E.P. Ippen, Appl. Phys. B **65**, 277 (1997)
4. F. Wang, A.G. Rozhin, V. Scardaci, Z. Sun, F. Hennrich, I.H. White, W.I. Milne, A.C. Ferrari, Nat. Nanotechnol. **3**, 738 (2008)
5. F. Shohda, M. Nakazawa, J. Mata, J. Tsukamoto, Opt. Express **18**, 9712 (2010)
6. N.H. Seong, D.Y. Kim, S.P. Veetil, Opt. Commun. **280**, 438 (2007)
7. K. Tamura, E.P. Ippen, H.A. Haus, L.E. Nelson, Opt. Lett. **18**, 1080 (1993)
8. D.Y. Tang, L.M. Zhao, Opt. Lett. **32**, 41 (2007)
9. I.N. Duling, Electron. Lett. **27**, 544 (1991)
10. A. Chong, J. Buckley, W. Renninger, F. Wise, Opt. Express **14**, 10095 (2006)
11. F.O. Ilday, J.R. Buckley, W.G. Clark, F.W. Wise, Phys. Rev. Lett. **92**, 4 (2004)
12. B. Oktem, C. Ulgudur, F.O. Ilday, Nat. Photon. **4**, 307 (2010)
13. H. Leblond, M. Salhi, A. Hideur, T. Chartier, M. Brunel, F. Sanchez, Phys. Rev. A **65** (2002)
14. B. Ortac, A. Hideur, M. Brunel, T. Chartier, M. Salhi, H. Leblond, F. Sanchez, Appl. Phys. B **77**, 589 (2003)
15. M.L. Dennis, I.N. Duling, IEEE J. Quantum Electron. **30**, 1469 (1994)
16. P.S. Hauge, F.H. Dill, Opt. Commun. **14**, 431 (1975)
17. R.M.A. Azzam, Opt. Acta **29**, 685 (1982)
18. S.M. Lee, W. Pan, C. Yang, Fiber Opt. Laser Sens. XIV **2839**, 133 (1996)
19. Y. Cui, R.M.A. Azzam, Opt. Lett. **21**, 89 (1996)
20. Y. Cui, R.M.A. Azzam, Rev. Sci. Instrum. **66**, 5552 (1995)
21. R.M.A. Azzam, A.G. Lopez, J. Opt. Soc. Am. A **6**, 1513 (1989)
22. M. Johnson, Appl. Opt. **18**, 1288 (1979)
23. T. Schreiber, B. Ortac, J. Limpert, A. Tünnermann, Opt. Express **15**, 8252 (2007)
24. B. Vodonos, A. Bekker, V. Smulakovsky, A. Gordon, O. Gat, N.K. Berger, B. Fischer, Opt. Lett. **30**, 2787 (2005)
25. H. Li, D.G. Ouzounov, F.W. Wise, Opt. Lett. **35**, 2403 (2010)